NANO · MICRO small
www.small-journal.com

Anchoring Group Mediated Radiolabeling for Achieving Robust Nanoimaging Probes

Lei Chen, Jianxian Ge, Baoxing Huang, Dandan Zhou, Gang Huang, Jianfeng Zeng, and Mingyuan Gao*

Radiolabeling counts for much in the functionalization of inorganic nanoparticles (NPs) because it endows NPs with high-sensitive imaging capacities apart from providing accurate pharmacokinetic information on the labeled particles, which makes the development of relevant radiolabeling chemistry highly desirable. Herein, a novel Ligand Anchoring Group MEdiated RAdioLabeling (LAGMERAL) method is reported, in which a polyethylene glycol (PEG) ligand with a diphosphonate (DP) terminal group plays a key role. It offers possibilities to radiolabel NPs through the spare coordination sites of the DP anchoring group. Through X-ray absorption spectroscopy studies, the coordination states of the foreign metal ions on the particle surface are investigated. In addition, radioactive Fe_3O_4 NPs are prepared by colabeling the particles with ^{125}I at the outskirt of the particles through a phenolic hydroxyl moiety of the PEG ligand, and ^{99m}Tc at the root of the ligand, respectively. In this way, the stabilities of these types of radiolabeling are compared both in vitro and in vivo to show the advantages of the LAGMERAL method. The outstanding stability of probe and simplicity of the labeling process make the current approach universal for creating advanced NPs with different combinations of functionalities of the inorganic NPs and radioactive properties of the metal radioisotopes.

1. Introduction

Functional inorganic nanoparticles (NPs) such as magnetic iron oxide NPs,[1–6] quantum dots,[7,8] rare-earth NPs,[9,10] noble-metal NPs,[11,12] and transition metal chalcogenide NPs[13] have shown great potentials for versatile biomedical applications. Their intrinsic physical properties allow not only for advanced imaging with remarkably improved precision, but also for beneficial combinations of different types of imaging modalities, and even the combination of diagnosis and therapies.[14–16] To this end, the radiolabeling of functional inorganic NPs is of clinical significance.[17–19] On the one hand, it provides accurate pharmacokinetic information about the functional NPs delivered into the body, and on the other hand it offers imaging capacities with extremely high sensitivity, quantifiable information, and unlimited penetration depth.[20,21] Therefore, a facile, reliable, rapid, and efficient method for the radiolabeling of NPs is essentially needed.

Generally, the methods for radiolabeling NPs can be divided into two categories, i.e., incorporating the radionuclides into the crystalline lattice of the inorganic nanocrystal core, and coupling the radionuclides on the surface of functional NPs via the secondary chelating moieties or specific moieties of particle surface capping agent. The former one is usually accomplished during the wet-chemical synthesis of NPs. For example, by introducing the corresponding radioactive precursors in the synthetic systems, ^{59}Fe-,[22,23] ^{68}Ga-,[24] ^{111}In-,[25] and ^{64}Cu-doped[26] superparamagnetic iron oxide NPs were successfully obtained by coprecipitation method, irrespective of the irregular shape and broad particle size polydispersity. Fortunately, the particles size distribution can remarkably be narrowed if the synthesis and in situ radioactive doping were carried out at high temperature through the thermal decomposition of metal precursors.[27] However, strict radiation protections are required through the whole synthetic process, which makes the experimental operations very laborious and thus limits the application of the aforementioned approaches.

Contrasting to in situ doping methods, radiolabeling through postsynthesis is apparently more convenient. Through isotopic exchange, monodisperse magnetic iron oxide NPs were obtained by incubating the oleate-capped particles with $^{59}FeCl_3$ in chloroform in the presence of free oleic acid.[28] Through absorption, iron oxide NPs stabilized by poly(acrylic acid) were successfully labeled with ^{69}Ge under ambient conditions.[29] In spite of the simplicity of these approaches, the room temperature reaction normally requires long time (≈24 h) to reach

L. Chen, J. X. Ge, B. X. Huang, D. D. Zhou, J. F. Zeng, M. Y. Gao
Center for Molecular Imaging and Nuclear Medicine
State Key Laboratory of Radiation Medicine and Protection
School for Radiological and Interdisciplinary Sciences (RAD-X)
Soochow University
Collaborative Innovation Center of Radiological Medicine of Jiangsu Higher Education Institutions
Suzhou 215123, China
E-mail: jfzeng@suda.edu.cn
G. Huang
Shanghai Key Laboratory of Molecular Imaging
Shanghai University of Medicine and Health Sciences
Shanghai 201318, China

The ORCID identification number(s) for the author(s) of this article can be found under https://doi.org/10.1002/smll.202104977.

DOI: 10.1002/smll.202104977

a satisfactory radiolabeling yield,[28,29] which is not compatible with short half-live radionuclides. More recently, elevating the radiolabeling temperature was demonstrated to be effective for accelerating the labeling process, e.g., ^{89}Zr-, ^{64}Cu-, and ^{111}In-labeled iron oxide particles were obtained within 1 h at 120 °C in sealed vials.[30–32] Nevertheless, this facile approach is apparently unsuitable for radiolabeling nanoprobes precoupled with biotargeting molecules such as antibody, because the latter will be deactivated under high temperature and pressure.

In comparison with the intrinsic radiolabeling, the extrinsic radiolabeling is preferred for constructing molecular imaging probes bearing versatile biovectors, because it can be carried out under mild conditions. For example, radioisotopes including ^{64}Cu,[33,34] ^{111}In,[35] ^{177}Lu,[36] and ^{68}Ga,[37,38] ^{125}I, and ^{131}I[39–41] were attached to the particle surface through the secondary chelating group of the particle ligand or tyrosine moiety specifically for iodine radioisotopes. Despite the obvious advantages of these established methods, the radiolabeling stability still challenges the extrinsic labeling approaches. Recent investigations showed that the radioisotope may be detached from the particle surface together the particle ligands in vivo,[25,28,35,42] leading to wrongful diagnosis. In this context, developing facile and reliable methods for radiolabeling functional NPs is of clinical translational relevance, but remains challenging with respect to radiochemistry.

Herein, we report a Ligand Anchoring Group MEdiated RAdioLabeling (LAGMERAL) method for effectively labeling functional inorganic NPs with metal radioisotopes. Previous studies have demonstrated that a polyethylene glycol (PEG) 2000 ligand bearing a diphosphonate (DP) moiety as anchoring group is very suitable for converting hydrophobic NPs into biocompatible ones. It is applicable not only for transition metal based NPs,[43] but also for lanthanides NPs,[44] and thus represents a universal ligand for the biomedical applications of these functional NPs. The multiple binding sites of the DP anchoring group also allow us to suppose that they may effectively entrap metal radioisotopes onto the surface of the functional NPs, distinctly different from the above-mentioned intrinsic and extrinsic radiolabeling approaches. To demonstrate this hypothesis, iron oxide NPs were chosen as a model particle. After surface PEGylation with DP-PEG, ^{99m}Tc labeling was carried out to rationally integrate the capacity for high spatial resolution of magnetic resonance imaging (MRI) with the high sensitivity of single-photon emission computed tomography (SPECT), simply by mixing the PEGylated iron oxide NPs with Na[^{99m}TcO$_4$]. To disclose the underlying molecular mechanism, X-ray absorption near-edge structure (XANES) and extended X-ray absorption fine structure (EXAFS) spectroscopy studies were performed to show the chemical state and coordination profiles of metal radionuclide ions on the surface of the labeled NPs. The results indicated that the metal ion at least bridged two DP groups, which further improved the binding affinity of the ligand to the particle surface. Thus, LAGMERAL represents an innovative method for radiolabeling of functional NPs toward versatile biomedical applications.

2. Results and Discussion

The hydrophobic Fe_3O_4 NPs as shown in Figure S1 (Supporting Information) were prepared through a conventional thermal decomposition method by using oleic acid as surface ligands. To render the as-prepared particles water-soluble and biocompatible, the DP-PEG ligand bearing a DP group at one end and a methoxy group at the other end of a PEG2000 chain was used to replace the hydrophobic ligand, as schematically shown in **Figure 1**a, to achieve DP-PEG coated Fe_3O_4 NPs (denoted

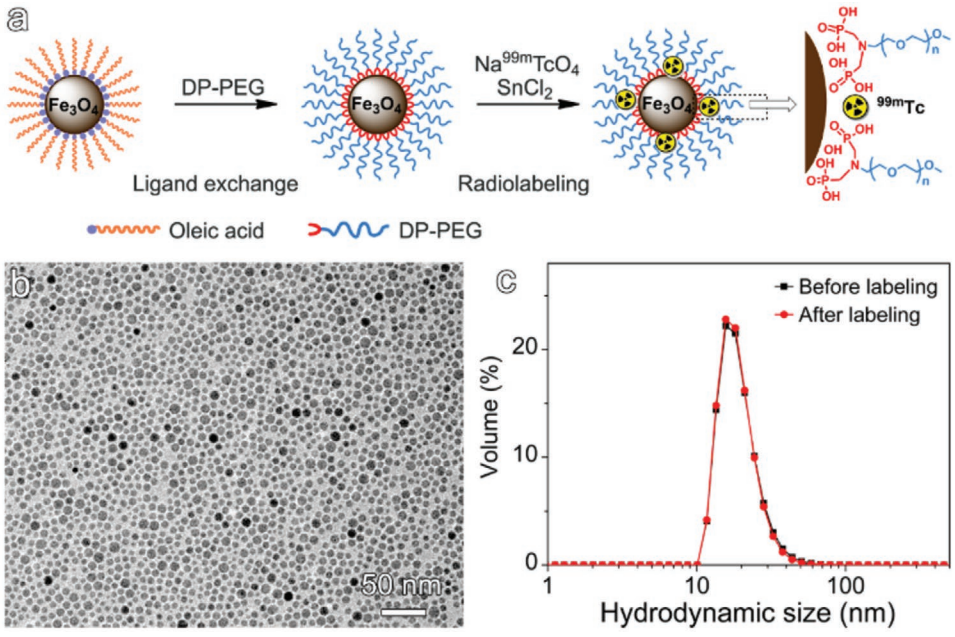

Figure 1. a) Schematic illustration of labeling DP-PEG coated Fe_3O_4 nanoparticles (NPs) through the diphosphonate (DP) anchoring group, b) a representative transmission electron microscopy (TEM) image of Fe_3O_4@DP-PEG NPs, and c) hydrodynamic size profiles of aqueous solutions of PEGylated Fe_3O_4 NPs recorded before and after ^{99m}Tc labeling.

as Fe_3O_4@DP-PEG). According to the transmission electron microscopy (TEM) image presented in Figure 1b, the average size of the resulting PEGylated particles was of 7.6 ± 1.2 nm. Further dynamic light scattering (DLS) studies revealed that the PEGylated Fe_3O_4 NPs are very colloidally stable in aqueous system due to the firm attachment of the DP-PEG ligands to the particle surface through the DP group (Figure S2, Supporting Information).

Apart from Fe^{3+} ion, the DP group can also firmly coordinate with many other types of metal ions.[45–48] In fact, phosphonate-functionalized compounds such as methylene DP (MDP) and ethylenediamine tetramethylene phosphonate (EDTMP) are used as the skeletal imaging agent in the clinic simply because they can firmly hold ^{99m}Tc apart from showing bone specificity.[49] It is then reasonable to speculate that DP-PEG coated iron oxide NPs can also be labeled with ^{99m}Tc through the spare –P–O$^-$ and –P=O moieties of the DP groups of the PEG ligand. To demonstrate this speculation, the PEGylated Fe_3O_4 NPs were mixed with Na[^{99m}TcO$_4$] in aqueous solution in the presence of $SnCl_2$. After 30 min incubation at room temperature, a labeling yield above 80% was achieved. In a huge contrast, the radiolabeling yield as low as 4.2% was achieved by a bare water-soluble 8 nm Fe_3O_4 nanoparticle prepared by slightly modifying a literature method with details given in Supporting Information, strongly supporting that the surface labeling of ^{99m}Tc is mediated by the bisphosphonate group. After being purified three times through ultrafiltration, a radiochemical purity up to 98.8% was achieved for the PEGylated Fe_3O_4 NPs. In addition, the ^{99m}Tc radiolabeling barely varies the hydrodynamic size profile of PEGylated Fe_3O_4 NPs as shown in Figure 1c. Most importantly, the resulting ^{99m}Tc-labeled Fe_3O_4 NPs (denoted as Fe_3O_4@^{99m}Tc-DP-PEG) exhibit excellent radiolabeling stability as shown in Figure S3 (Supporting Information). Specifically, only 12% of the labeled ^{99m}Tc ions were detached from Fe_3O_4 NPs after they were incubated in fetal bovine serum (FBS) for 24 h.

All these features indicate that the LAGMERAL approach enjoys superiority over the other labeling methods. Nevertheless, the underlying labeling mechanisms remain to be investigated. To show the detailed coordination situation of ^{99m}Tc ions, Ga^{3+} was adopted instead of ^{99m}Tc^{4+} to prepare an analogue of Fe_3O_4@^{99m}Tc-DP-PEG particles, i.e., Fe_3O_4@Ga-DP-PEG, as Ga^{3+} can easily be obtained and characterized through XANES and EXAFS.[50,51] According to the XANES spectra shown in **Figure 2**a, Fe_3O_4@Ga-DP-PEG presents a Ga K-edge very close to Ga_2O_3 rather than Ga foil at ≈10 367 eV, indicating the valance state of Ga atoms in Fe_3O_4@Ga-DP-PEG is +3. However, the k^3-weighted EXAFS spectra describing the superposition of backscattering atoms' signals (Figure 2b) reveal that the amplitude of Ga signal from Fe_3O_4@Ga-DP-PEG is greater than that of Ga_2O_3 in the low-wave region, implying that there exists low Z atom in the second shell. Because Ga^{3+} can only bind with O in the first shell, it is reasonable to attribute the low Z element in the Fe_3O_4@Ga-DP-PEG to the phosphorus atom as it is next to the oxygen atom binding with Ga.

The coordination environment of Ga atoms in Fe_3O_4@Ga-DP-PEG was further elucidated through Fourier transform (FT) analyses of the EXAFS spectra. As shown in Figure 2c, the FT-EXAFS spectrum of Fe_3O_4@Ga-DP-PEG in R space shows two

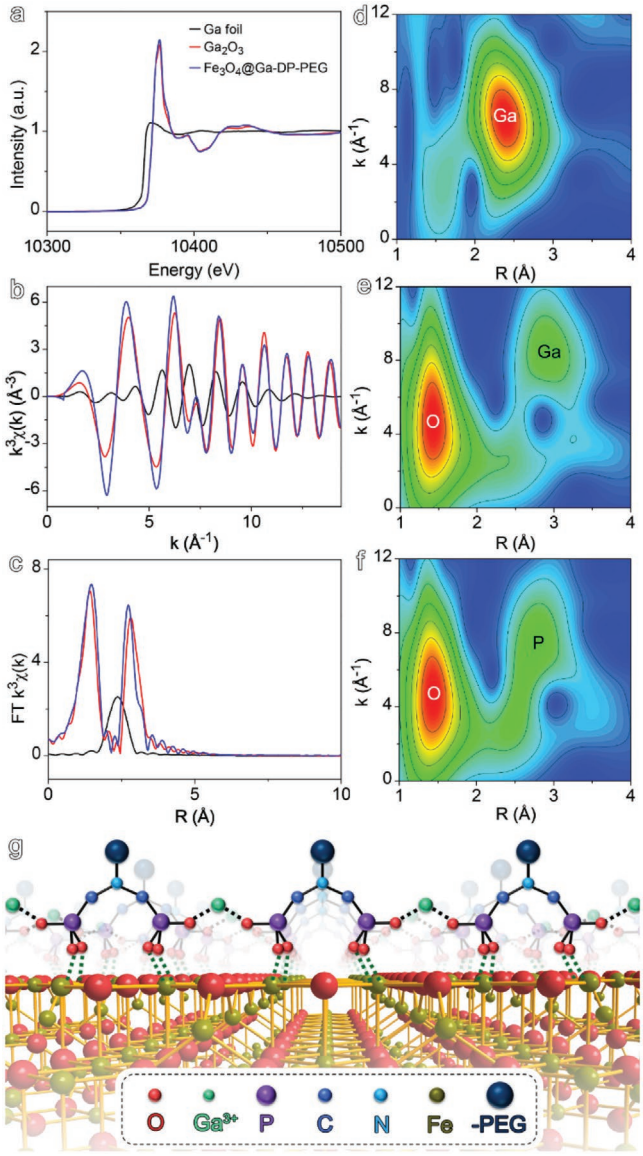

Figure 2. Ga K-edge X-ray absorption near-edge structure (XANES) spectra (a), k^3-weighted EXAFS spectra (b), and Fourier transformed k^3-weighted χ(k)-functions of the EXAFS spectra of Ga foil, Ga_2O_3, and Fe_3O_4@Ga-DP-PEG (c), together with wavelet transforms of the k^3-weighted extended X-ray absorption fine structure (EXAFS) spectra for Ga foil (d), Ga_2O_3 (e), and Fe_3O_4@Ga-DP-PEG (f). The cross-linking effect of Ga^{3+} on the DP-PEG ligands anchoring on the surface of Fe_3O_4 nanoparticles (NPs) is schematically shown (g).

strong shells at 1.4 and 2.7 Å, respectively, indicating that there are one or more types of atoms at these distances. The backscattering atoms can be more clearly distinguished from the three-dimensional coordination structures obtained by the EXAFS wavelet transform analysis to show the intensity maximum position in the second shell. According to the results shown in Figure 2d–f, Ga foil presents no second shell atoms as expected. In difference, both Fe_3O_4@Ga-DP-PEG and Ga_2O_3 present second shell atoms, but in slightly different positions, which is supportive to the attribution of the second shell atoms in Fe_3O_4@Ga-DP-PEG to P. To provide more detailed information

about the second shell, the R space data given in Figure 2c were further analyzed with Athena software according to the basic formula of EXAFS. According to the fitting results provided in Table S1 (Supporting Information), the ratio between the second shell P and Ga in Fe_3O_4@Ga-DP-PEG is approximately 3.3:1. As each DP-PEG molecule possesses only two phosphorus atoms, the above results indicate that each Ga^{3+} ion in the Fe_3O_4@Ga-DP-PEG binds at least with two DP-PEG ligands. In other words, DP-PEG ligands anchoring on the particles surface can be cross-linked by Ga^{3+} ions as schematically shown in Figure 2g.

The binding affinity of a given ligand will definitely affect the colloidal stability of the underlying particles and the radiolabeling stability as well, if the radionuclide is extrinsically labeled. As shown in Figure 2g, the radionuclide can bind with the DP anchoring groups from adjacent PEG molecules, which apparently increases the denticity of bridged PEG ligands as a whole. Therefore, it is reasonable to expect that the bridging effect of the foreign metal ions will consequently increase the binding affinity of the PEG ligands. To verify this hypothesis, ^{125}I was adopted to label the DP-PEG ligand on the opposite side of the DP group for detecting the binding stability of ligand through ^{125}I signal. In detail, a PEG ligand bearing a DP group at one end and a maleimide group at the other end of PEG2000 chain (denoted as DP-PEG-Mal) was used to PEGylate the Fe_3O_4 NPs. Then, 4-mercaptophenol was conjugated to the PEGylated NPs through a click reaction between thiol group and maleimide group to covalently attach a phenolic hydroxyl moiety on the particle surface, through which the resulting PEGylated particles were radiolabeled with ^{125}I via the commonly used chloramine-T method. The detailed procedures are shown in **Figure 3**a. After purification, a radiolabeling yield of ≈60% and radiochemical purity of 98.5% were obtained for resulting particles denoted as Fe_3O_4@DP-PEG-^{125}I. Owing to the excellent colloidal stability benefited from the PEG ligands anchored through the DP group, the radiolabeling process and the following purification through multiple ultrafiltration did not lead to evident change to the hydrodynamic size profile of the PEGylated Fe_3O_4 NPs (Figure 3b). The results shown in Figure 3c and Figure S4 (Supporting Information) reveal that the binding stability of the DP ligand in Fe_3O_4@DP-PEG-^{125}I can remarkably be improved upon introduction of Ga^{3+} coordination. Specifically, about 23.8% of the surface ligands will be detached after Fe_3O_4@DP-PEG-^{125}I particles are stored in water for 24 h, according to the signal of the ^{125}I-labeled PEG ligand in the filtrate. However, this number is decreased to a few percent if Ga^{3+} bridging is preintroduced. Therefore, it can be concluded that the introduction of foreign metal ions helps stabilize the surface ligand as well as the radiolabels introduced through extrinsic approach.

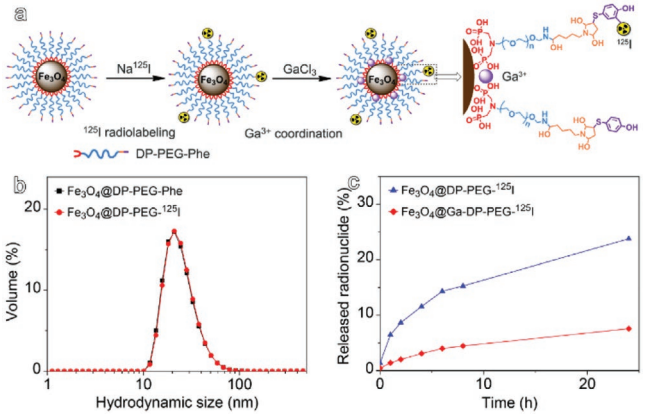

Figure 3. Schematic illustration for showing the procedures for labeling Fe_3O_4 nanoparticles (NPs) with ^{125}I followed by the coordination of Ga^{3+} with the spare binding sites of anchoring diphosphonate (DP) groups (a), hydrodynamic size profiles of the PEGylated particles before (Fe_3O_4@DP-PEG-Phe) and after (Fe_3O_4@DP-PEG-^{125}I) iodine labeling (b), together with the ligand binding stability results for showing the difference between Fe_3O_4@DP-PEG-^{125}I and Fe_3O_4@Ga-DP-PEG-^{125}I in pure water (c).

To further discover the advantages of LAGMERAL method in achieving stable radiolabeled nanoprobes, healthy BALB/c mouse was chosen as animal model to show the stability of differently radiolabeled NPs in vivo. Apart from the ^{125}I-labeled and ^{99m}Tc-labeled Fe_3O_4 NPs, Fe_3O_4 NPs sequentially labeled with ^{125}I and ^{99m}Tc (denoted as Fe_3O_4@^{99m}Tc-DP-PEG-^{125}I) were prepared. After purification, the resulting Fe_3O_4@^{99m}Tc-DP-PEG-^{125}I containing 200 μg Fe, 600 μCi ^{125}I, and 2000 μCi ^{99m}Tc (corresponding to 10 mg Fe, 30 mCi ^{125}I, and 100 mCi ^{99m}Tc per kilogram body weight) was intravenously injected into healthy mice that were subsequently subjected to SPECT-CT imaging. As the emissions of ^{125}I and ^{99m}Tc are located at 31 and 140 KeV, respectively, they can be well resolved by energy discriminant detectors for independent reconstruction (Figure S5, Supporting Information). As shown in **Figure 4**a,b, the biodistributions of ^{125}I and ^{99m}Tc signals are similar in some organs while significantly different in the others. Specifically, during the initial stage, both ^{125}I and ^{99m}Tc signals are highly distributed in blood pool, as evidenced by the strong signal from the heart. With the lapse of time, ^{125}I gradually escapes the blood system and becomes gradually accumulated in bladder, stomach, thyroid, and mammary gland, which is quite different from the general pharmacokinetics behaviors of nanomaterials that generally exhibit a quick and high uptake by RES organs including liver and spleen. However, through the ^{99m}Tc signal channel, only negligible signals are presented from thyroid, stomach, and mammary gland over the whole observation time period, contrasting to ^{125}I signals.

To understand these behaviors, the biodistribution based on ^{125}I and ^{99m}Tc was quantified by extracting the signals from the volume of interest (VOI) of desired organs or tissues, and expressed by percentage of the injected dose (%ID) or percentage of the injected dose per gram (%ID/g). As shown in Figure 4c–j, ^{125}I and ^{99m}Tc present consistent pharmacokinetic profiles for heart and lung, suggesting that Fe_3O_4@^{99m}Tc-DP-PEG-^{125}I can well keep its integrity in the blood stream. This was evidenced by the facts that both Fe_3O_4@DP-PEG-^{125}I and Fe_3O_4@^{99m}Tc-DP-PEG exhibited high radiolabeling stability in FBS even after 8 h incubation. According to the fitting results obtained through a pharmacokinetic two-compartment model, as indicated in Figure S6 (Supporting Information), the distribution half-life and elimination half-life of the radiolabeled NPs are 9.3 and 263.3 min, respectively. Apart from heart and lung, ^{99m}Tc signals present time-dependent behaviors similar to ^{125}I signals with reversed tendencies for kidney and bladder, but with higher signal levels particularly for kidney. According to

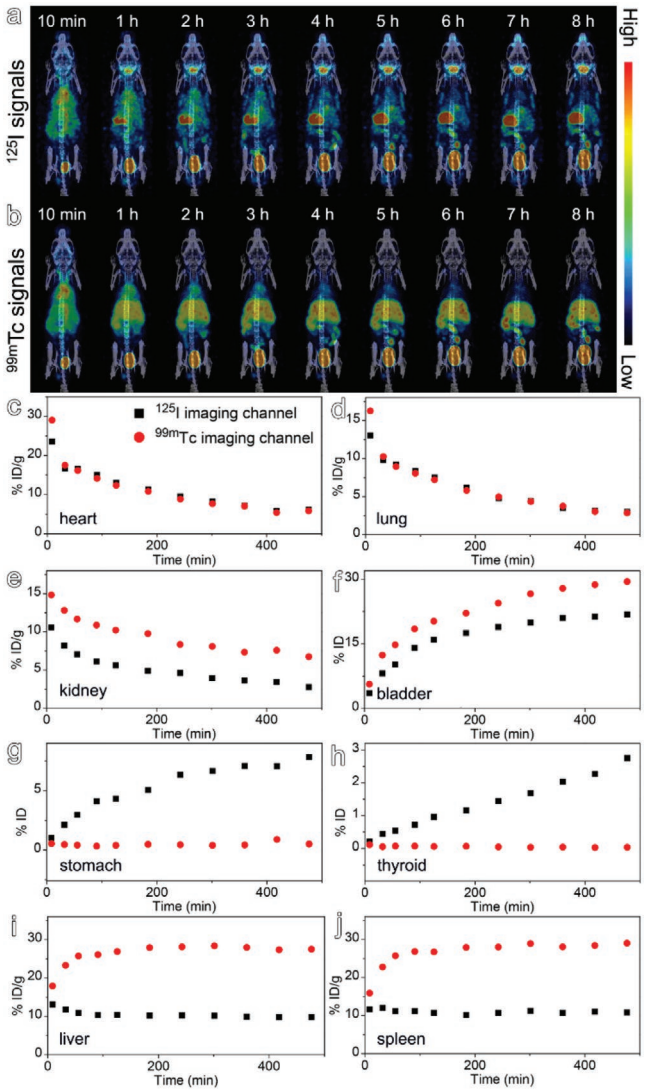

Figure 4. Single-photon emission computed tomography (SPECT)/CT images of mouse intravenously injected with Fe_3O_4@^{99m}Tc-DP-PEG-^{125}I acquired through ^{125}I imaging channel (a) and ^{99m}Tc imaging channel (b), respectively, together with the time distribution acquired by ^{125}I and ^{99m}Tc signals in different organs such as heart (c), lung (d), kidney (e), bladder (f), stomach (g), thyroid (h), liver (i), and spleen (j).

the ^{99m}Tc signal, the particle accumulation in bladder is close to 30%ID 8 h postinjection, which is much higher than the dissociation rate of ^{99m}Tc (≈9.0%) determined in FBS, suggesting that some of the administrated Fe_3O_4@^{99m}Tc-DP-PEG-^{125}I particles are excreted via the renal clearance pathway.[44]

Apart from these similar pharmacokinetic behaviors, there are also a number of differences between ^{125}I and ^{99m}Tc signal patterns. For example, the ^{125}I signals from stomach and thyroid keep increasing to reach 7.8 and 2.7%ID 8 h postinjection, respectively, while ^{99m}Tc signals of these two organs keep nearly constant. It was demonstrated that the above ^{125}I signal patterns were very close to the pharmacokinetics behaviors of free ^{125}I and ^{125}I-PEG as shown in Figure S7a,b (Supporting Information). It can therefore be concluded that the distribution of the particles indicated by the ^{125}I signal is strongly interfered by the released ^{125}I owing to continuous deiodination in vivo. In addition, ^{99m}Tc signals of liver and spleen quickly increase during the initial 3 h postinjection and then become stabilized, while the ^{125}I signals from these two organs slightly decrease during the early stage and then maintain at low levels around 10% during the whole time period. The discrepancy of ^{99m}Tc and ^{125}I signals from these organs can be understood by the facts that the deiodinases that are indispensable enzymes for deiodination are mainly located in organs such as liver,[52] and the proteolytic enzymes that can detach the particle surface ligand also are populated in liver, spleen, etc.[42] In consequence, the particle accumulations in these two organs are underestimated according to ^{125}I signal. Fortunately, particle distributions in liver and spleen depicted by ^{99m}Tc are well consistent with those determined through inductively coupled plasma mass spectrometry,[44] suggesting that the ^{99m}Tc labeling is rather stable and reliable in vivo. Therefore, it can be concluded that LAGMERAL method is very suitable for radiolabeling NPs for tracing their in vivo distributions. To further show the bridging effect of given foreign metal ion can increase the binding affinity of the PEG ligands in vivo, the pharmacokinetic behaviors of Fe_3O_4@Ga-DP-PEG-^{125}I and Fe_3O_4@DP-PEG-^{125}I were also recorded. The results given in Figure S8 (Supporting Information) indicated that the Ga^{3+} coordination effectively improved the binding stability of the PEG ligand in vivo, as Fe_3O_4@Ga-DP-PEG-^{125}I presented a much higher liver signal than Fe_3O_4@DP-PEG-^{125}I, which helps suppress the false signal if the radioisotopes of iodine are needed to be radiolabeled extrinsically.

In fact, the extrinsic radiolabeling is widely used for creating molecular imaging probes through macrocyclic chelators, e.g., DOTA and NOTA. With respect to nanoimaging probes, these chelators are typically positioned at the outskirt of NPs, the following chelation with metal radioisotopes is prone to alter the surface charge, hydrophilicity of NPs, and hydrodynamic properties, which may lead to unexpected biodistribution in vivo. In contrast, the current LAGMERAL approach innovatively positions the radiometal ions at root of the particle ligands, which can minimize the effects of the radiolabeling on the nanoimaging probes with preoptimized properties, apart from its facileness. In addition, the spare surface phosphate moieties are universal for binding with the commonly used radioisotopes including ^{59}Fe, ^{111}In, ^{64}Cu, ^{90}Y, ^{68}Ga, and ^{177}Lu, apart from ^{99m}Tc.

3. Conclusion

In summary, a universal Ligand Anchoring Group MEdiated RAdioLabeling (LAGMERAL) method for labeling functional inorganic NPs with metal radioisotopes has been developed. The X-ray absorption spectroscopy studies reveal that the foreign (radio)metal ion cross-links the ligands through the unique DP anchoring groups, leading to robust radiolabeling owing to the enhanced the binding affinity of the ligands. Different from intrinsic and extrinsic labeling approaches, the current LAGMERAL method position the radiometal ions at the root of the particle ligands, which is practically advisable for labeling nanoprobes without altering their preoptimized properties and thus represents an innovative approach for creating

novel multifunctional nanoprobes for theranostic applications apart from showing the pharmacokinetic behaviors of the labeled particles. In addition, to the best of our knowledge, this is the first report of using the indispensable anchoring group of particle surface ligands to achieve stable radiolabeling. This work is our first step in the development of clinically translational multimodal imaging agents. Future work for expanding different kinds of radionuclides, NPs, targeting imaging agents, and kit development is undergoing. We thus believe that the radiolabeling method developed herein has profound implications in the field of nanomedicine.

Supporting Information

Supporting Information is available from the Wiley Online Library or from the author.

Acknowledgements

The authors thank for the financial support from the National Key Research and Development Program of China (2018YFA0208800), the National Natural Science Foundation of China (81720108024), Nature Science Foundation of Jiangsu Higher Education Institutions of China (20KJA150006), the Natural Science Foundation of Jiangsu Province (BK20191418), the Suzhou Key Industry Technology Innovation Pro-jects (SYG202036), Postgraduate Research & Practice Innovation Pro-gram of Jiangsu Province (KYCX20_2682), and Priority Academic Program Development of Jiangsu Higher Education Institutions (PAPD).

Conflict of interest

The authors declare no conflict of interest.

Data Availability Statement

Research data are not shared.

Keywords

anchoring group, coordination, iron oxide nanoparticle, metal radioisotope, radiolabeling stability

Received: August 18, 2021
Revised: August 29, 2021
Published online:

[1] J. Zeng, L. Jing, Y. Hou, M. Jiao, R. Qiao, Q. Jia, C. Liu, F. Fang, H. Lei, M. Gao, *Adv. Mater.* **2014**, *26*, 2694.
[2] F. Li, Z. Liang, J. Liu, J. Sun, X. Hu, M. Zhao, J. Liu, R. Bai, D. Kim, X. Sun, T. Hyeon, D. Ling, *Nano Lett.* **2019**, *19*, 4213.
[3] H. Wei, O. Bruns, M. Kaul, E. Hansen, M. Barch, A. Wisniowska, O. Chen, Y. Chen, N. Li, S. Okada, J. Cordero, M. Heine, C. Farrar, D. Montana, G. Adam, H. Ittrich, A. Jasanoff, P. Nielsen, M. Bawendi, *Proc. Natl. Acad. Sci. USA* **2017**, *114*, 2325.
[4] Y. Lu, Y. Xu, G. Zhang, D. Ling, M. Wang, Y. Zhou, Y. Wu, T. Wu, M. Hackett, B. Kim, H. Chang, J. Kim, X. Hu, L. Dong, N. Lee, F. Li, J. He, L. Zhang, H. Wen, S. C. B. Yang, T. Hyeon, D. Zou, *Nat. Biomed. Eng.* **2017**, *1*, 637.
[5] C. Liang, X. Zhang, X. Z. Cheng, M. Yang, W. Huang, X. Dong, *View* **2020**, *1*, 20200046.
[6] R. Zhang, B. Le, W. Xu, K. Guo, X. Sun, H. Su, L. Huang, J. Huang, T. Shen, T. Liao, Y. Liang, J. X. J. Zhang, H. Dai, K. Qian, *Small Methods* **2019**, *3*, 1800474.
[7] Z. Ma, F. Wang, Y. Zhong, F. Salazar, J. Li, M. Zhang, F. Ren, A. Wu, H. Dai, *Angew. Chem., Int. Ed.* **2020**, *59*, 20552.
[8] L. Ye, K. Yong, L. Liu, I. Roy, R. Hu, J. Zhu, H. Cai, W. Law, J. Liu, K. Wang, J. Liu, Y. Liu, Y. Hu, X. Zhang, M. Swihart, P. Prasad, *Nat. Nanotechnol.* **2012**, *7*, 453.
[9] D. Naczynski, M. Tan, M. Zevon, B. Wall, J. Kohl, A. Kulesa, S. Chen, C. Roth, R. Riman, P. Moghe, *Nat. Commun.* **2013**, *4*, 2199.
[10] Y. Hou, R. Qiao, F. Fang, X. Wang, C. Dong, K. Liu, C. Liu, Z. Liu, H. Lei, F. Wang, M. Gao, *ACS Nano* **2013**, *7*, 330.
[11] J. Yang, R. Wang, L. Huang, M. Zhang, J. Niu, C. Bao, N. Shen, M. Dai, Q. Guo, Q. Wang, Q. Wang, Q. Fu, K. Qian, *Angew. Chem., Int. Ed.* **2020**, *59*, 1703.
[12] J. Cao, X. Shi, D. D. Gurav, L. Huang, H. Su, K. Li, J. Niu, M. Zhang, Q. Wang, M. Jiang, K. Qian, *Adv. Mater.* **2020**, *32*, 2000906.
[13] S. Zhang, C. Sun, J. Zeng, Q. Sun, G. Wang, Y. Wang, Y. Wu, S. Dou, M. Gao, Z. Li, *Adv. Mater.* **2016**, *28*, 8927.
[14] D. Kim, J. Kim, Y. Park, N. Lee, T. Hyeon, *ACS Cent. Sci.* **2018**, *4*, 324.
[15] B. R. Smith, S. S. Gambhir, *Chem. Rev.* **2017**, *117*, 901.
[16] L. Jing, C. Yang, P. Zhang, J. Zeng, Z. Li, M. Gao, *View* **2020**, *1*, e19.
[17] P. Bouziotis, D. Psimadas, T. Tsotakos, D. Stamopoulos, C. Tsoukalas, *Curr. Top. Med. Chem.* **2012**, *12*, 2694.
[18] J. Lamb, J. P. Holland, *J. Nucl. Med.* **2018**, *59*, 382.
[19] J. Ge, Q. Zhang, J. Zeng, Z. Gu, M. Gao, *Biomaterials* **2020**, *228*, 119553.
[20] C. T. Yang, K. K. Ghosh, P. Padmanabhan, O. Langer, J. Liu, D. N. C. Eng, C. Halldin, B. Gulyas, *Theranostics* **2018**, *8*, 6210.
[21] C. Perez-Medina, A. J. P. Teunissen, E. Kluza, W. J. M. Mulder, R. van der Meel, *Adv. Drug Delivery Rev.* **2020**, *154–155*, 123.
[22] R. Weissleder, D. D. Stark, B. L. Engelstad, B. R. Bacon, C. C. Compton, D. L. White, P. Jacobs, J. Lewis, *Am. J. Roentgenol.* **1989**, *152*, 167.
[23] S. Majumdar, S. S. Zoghbi, J. C. Gore, *Invest. Radiol.* **1990**, *25*, 771.
[24] J. Pellico, J. Ruiz-Cabello, M. Saiz-Alia, G. Del Rosario, S. Caja, M. Montoya, L. Fernandez de Manuel, M. P. Morales, L. Gutierrez, B. Galiana, J. A. Enriquez, F. Herranz, *Contrast Media Mol. Imaging* **2016**, *11*, 203.
[25] J. Llop, P. Jiang, M. Marradi, V. Gomez-Vallejo, M. Echeverria, S. Yu, M. Puigivila, Z. Baz, B. Szczupak, C. Perez-Campana, Z. Mao, C. Gao, S. E. Moya, *J. Mater. Chem. B* **2015**, *3*, 6293.
[26] R. M. Wong, D. A. Gilbert, K. Liu, A. Y. Louie, *ACS Nano* **2012**, *6*, 3461.
[27] J. Zeng, B. Jia, R. Qiao, C. Wang, L. Jing, F. Wang, M. Gao, *Chem. Commun.* **2014**, *50*, 2170.
[28] B. Freund, B. U. I. Tromsdorf, O. T. Bruns, M. Heine, A. Giemsa, A. Bartelt, S. C. Salmen, N. Raabe, J. Heeren, H. Ittrich, R. Reimer, H. Hohenberg, U. Schumacher, H. Weller, P. Nielsen, *ACS Nano* **2012**, *6*, 7318.
[29] R. Chakravarty, H. F. Valdovinos, F. Chen, C. M. Lewis, P. A. Ellison, H. Luo, M. E. Meyerand, R. J. Nickles, W. Cai, *Adv. Mater.* **2014**, *26*, 5119.
[30] E. Boros, A. M. Bowen, L. Josephson, N. Vasdev, J. P. Holland, *Chem. Sci.* **2015**, *6*, 225.
[31] H. Yuan, M. Q. Wilks, M. D. Normandin, G. El Fakhri, C. Kaittanis, L. Josephson, *Nat. Protoc.* **2018**, *13*, 392.
[32] M. D. Normandin, H. Yuan, M. Q. Wilks, H. H. Chen, J. M. Kinsella, H. Cho, N. J. Guehl, N. Absi-Halabi, S. M. Hosseini, G. El Fakhri, D. E. Sosnovik, L. Josephson, *Angew. Chem., Int. Ed.* **2015**, *54*, 13002.

[33] C. Glaus, R. Rossin, M. J. Welch, G. Bao, *Bioconjugate Chem.* **2010**, *21*, 715.
[34] H. Y. Lee, Z. Li, K. Chen, A. R. Hsu, C. Xu, J. Xie, S. Sun, X. Chen, *J. Nucl. Med.* **2008**, *49*, 1371.
[35] H. Wang, R. Kumar, D. Nagesha, R. I. Duclos, S. Sridhar, S. J. Gatley, *Nucl. Med. Biol.* **2015**, *42*, 65.
[36] S. Shanehsazzadeh, C. Grüttner, H. Yousefnia, A. Lahooti, A. Gholami, S. Nosrati, S. Zolghadri, S. H. M. Anijdan, A. Lotfabadi, B. Shiri Varnamkhasti, F. J. Daha, A. R. Jalilian, *Radiochim. Acta* **2016**, *104*, 337.
[37] B. P. Burke, N. Baghdadi, G. S. Clemente, N. Camus, A. Guillou, A. E. Kownacka, J. Domarkas, Z. Halime, R. Tripier, S. J. Archibald, *Faraday Discuss.* **2014**, *175*, 59.
[38] B.-B. Cho, J. H. Park, S. J. Jung, J. Lee, J. H. Lee, M. G. Hur, C. Justin Raj, K.-H. Yu, *J. Radioanal. Nucl. Chem.* **2015**, *305*, 169.
[39] S. Liu, B. Jia, R. Qiao, Z. Yang, Z. Yu, Z. Liu, K. Liu, J. Shi, H. Ouyang, F. Wang, M. Gao, *Mol. Pharmaceutics* **2009**, *6*, 1074.
[40] Y. Zhao, M. Liang, X. Li, K. Fan, J. Xiao, Y. Li, H. Shi, F. Wang, H. S. Choi, D. Cheng, X. Yan, *ACS Nano* **2016**, *10*, 4184.
[41] J. Wang, H. Zhao, Z. Zhou, P. Zhou, Y. Yan, M. Wang, H. Yang, Y. Zhang, S. Yang, *ACS Appl. Mater. Interfaces* **2016**, *8*, 19872.
[42] W. G. Kreyling, A. M. Abdelmonem, Z. Ali, F. Alves, M. Geiser, N. Haberl, R. Hartmann, S. Hirn, D. J. de Aberasturi, K. Kantner, G. Khadem-Saba, J. M. Montenegro, J. Rejman, T. Rojo, I. R. de Larramendi, R. Ufartes, A. Wenk, W. J. Parak, *Nat. Nanotechnol.* **2015**, *10*, 619.
[43] Z. Gao, Y. Hou, J. Zeng, L. Chen, C. Liu, W. Yang, M. Gao, *Adv. Mater.* **2017**, *29*, 1701095.
[44] C. Liu, Z. Gao, J. Zeng, Y. Hou, F. Fang, Y. Li, R. Qiao, L. Shen, H. Lei, W. Yang, M. Gao, *ACS Nano* **2013**, *7*, 7227.
[45] M. Jiao, L. Jing, C. Liu, Y. Hou, J. Huang, X. Wei, M. Gao, *Chem. Commun.* **2016**, *52*, 5872.
[46] R. Torres Martin de Rosales, R. Tavare, A. Glaria, G. Varma, A. Protti, P. J. Blower, *Bioconjugate Chem.* **2011**, *22*, 455.
[47] J. Peng, Y. Sun, L. Zhao, Y. Wu, W. Feng, Y. Gao, F. Li, *Biomaterials* **2013**, *34*, 9535.
[48] L. Sandiford, A. Phinikaridou, A. Protti, L. K. Meszaros, X. Cui, Y. Yan, G. Frodsham, P. A. Williamson, N. Gaddum, R. M. Botnar, P. J. Blower, M. A. Green, R. T. de Rosales, *ACS Nano* **2013**, *7*, 500.
[49] S. Banerjee, G. Samuel, K. Kothari, P. R. Unni, H. D. Sarma, M. R. A. Pillai, *Nucl. Med. Biol.* **2001**, *28*, 205.
[50] B. Qiao, A. Wang, X. Yang, L. F. Allard, Z. Jiang, Y. Cui, J. Liu, J. Li, T. Zhang, *Nat. Chem.* **2011**, *3*, 634.
[51] B. Ravel, M. Newville, *J. Synchrotron Radiat.* **2005**, *12*, 537.
[52] K. Richard, R. Hume, E. Kaptein, J. P. Sanders, H. van Toor, W. W. De Herder, J. C. den Hollander, E. P. Krenning, T. J. Visser, *J. Clin. Endocrinol. Metab.* **1998**, *83*, 2868.